International Journal of Advanced Technology in Engineering and Science
Vol. No. 14, Issue No. 06, June 2026
www.ijates.com
ijates
ISSN 2348 - 7550

Transient Thermal Response and Recovery Dynamics of Hybrid Phase Change Material-Heat Pipe Cooling Systems Under Intermittent Heat Loads: A Numerical Study

Raviteja Mommileti[1], Rambabu Dara[2],

SDVVS Bhimeshwar Reddy[3], Adduri S S M Sitaramamurty[4]

[1,2,3,4] Department of Mechanical Engineering, Aditya University, Aditya Nagar, ADB Rd, Surampalem, Andhra Pradesh 533437

**Corresponding author email: ravimommileti096@gmail.com*

Highlights

- A reduced-order numerical framework is developed for hybrid PCM-heat pipe cooling under intermittent thermal loads.
- PCM enthalpy modelling is coupled with an effective heat-pipe thermal resistance model.
- Hybrid cooling reduces source peak temperature compared with heat-pipe-only and PCM-only configurations.
- Thermal lag, recovery time, melt fraction and energy partition are introduced as design metrics.
- Long-duration simulations identify cyclic heat accumulation and PCM utilisation limits.

Abstract

Intermittent heat generation is common in compact electronic, power electronic and energy-storage systems, where transient power spikes can produce short-duration thermal overshoots that are not fully captured by steady-state thermal design methods. Phase change materials (PCMs) provide passive thermal buffering through latent heat absorption, while heat pipes offer high effective heat-transfer capability between localised evaporator and condenser regions. However, the coupled transient behaviour of PCM-heat pipe systems under repeated heating and recovery cycles remains insufficiently quantified, particularly with respect to thermal lag, recovery time, incomplete PCM resolidification, and cyclic energy redistribution. This study presents a purely numerical investigation of a hybrid PCM-heat pipe cooling system subjected to deterministic and stochastic intermittent heat loads. A SolidWorks-derived geometry is represented using a reduced-order thermal resistance-capacitance model, while PCM melting and solidification are described using an enthalpy-based formulation. Heat pipe performance is represented using an effective thermal resistance calibrated against manufacturer- or reference-provided heat-pipe data. The numerical model is further checked using a Stefan-type phase-change benchmark. Four configurations are compared: heat-pipe-only, PCM-only, hybrid PCM-heat-pipe, and enhanced hybrid PCM-heat-pipe. The calibrated numerical results show that the heat-pipe-only system reaches a maximum

source temperature of 77.02 °C, while the hybrid and enhanced hybrid configurations reduce the peak temperature to 64.20 °C and 61.79 °C, respectively, under the reference intermittent load profile. The PCM-only case shows severe heat accumulation, reaching 155.51 °C, because stored heat is not removed efficiently during off-periods. The results demonstrate that hybridisation is beneficial only when latent heat storage is combined with sufficient heat rejection capacity. The proposed framework provides a design tool for evaluating passive hybrid thermal management systems under realistic time-varying thermal loads.

Keywords-*Phase change material; heat pipe; intermittent heat load; transient thermal management; enthalpy method; thermal lag; recovery time.*

Nomenclature

Symbol	Description	Unit
A	Heat-transfer area	m^2
C_i	Thermal capacitance of node i	$J\ K^{-1}$
c_p	Specific heat capacity	$J\ kg^{-1}\ K^{-1}$
D	Duty cycle	-
E_{in}	Total input thermal energy	J
E_{latent}	Latent energy stored in PCM	J
$E_{removed}$	Heat removed through condenser	J
f_m	PCM melt fraction	-
h	Convective heat-transfer coefficient	$W\ m^{-2}\ K^{-1}$
H	Specific enthalpy of PCM	$J\ kg^{-1}$
k	Thermal conductivity	$W\ m^{-1}\ K^{-1}$
L	Latent heat of fusion	$J\ kg^{-1}$
P	Heat-load period	s
Q(t)	Time-dependent heat input	W
Q_{max}	Maximum heat-pipe heat transport capacity	W
R_{cond}	Conductive thermal resistance	$K\ W^{-1}$
R_{conv}	Convective thermal resistance	$K\ W^{-1}$
$R_{hp,eff}$	Effective heat-pipe thermal resistance	$K\ W^{-1}$
T_s	Heat source temperature	°C
T_b	Base plate temperature	°C
T_e	Heat-pipe evaporator temperature	°C
T_c	Heat-pipe condenser temperature	°C
T_{pcm}	PCM temperature	°C
T_{inf}	Ambient temperature	°C

T_{max}	Maximum source temperature	°C
tau_{lag}	Thermal lag	s
tau_{rec}	Recovery time	s
rho	Density	kg m^{-3}

1. Introduction

The thermal management of compact electronic, power electronic, and energy-storage systems is increasingly governed by transient rather than steady-state heat generation. Unlike conventional steady-state thermal loading, modern electronic packages, embedded controllers, battery modules, pulsed power devices and intermittent-duty power converters frequently operate through repeated transitions between idle, moderate and peak power states. These thermal pulses can generate short-duration source-temperature overshoots, delayed heat spreading, incomplete thermal recovery, and cycle-to-cycle heat accumulation. In such systems, the maximum temperature is not determined solely by the average heat-generation rate, but also by the timing, duration, amplitude, and recovery interval of heat pulses. Consequently, thermal management strategies designed solely for steady-state heat dissipation may underestimate the severity of transient temperature excursions and fail to predict whether a cooling system can return to a safe thermal state before the next power pulse begins.

Passive thermal management technologies remain attractive for compact systems because they do not require complex control, external pumping power or active feedback hardware. Among these approaches, phase change materials (PCMs) are widely investigated because they absorb thermal energy through latent heat during melting, thereby delaying temperature rise over a relatively narrow temperature interval. PCM-based heat sinks have been shown to improve transient thermal performance in electronic devices, particularly before complete melting occurs. Kandasamy, Wang and Mujumdar (2008) experimentally and numerically investigated PCM-based heat sinks for electronic cooling and demonstrated that the inclusion of PCM can reduce the die junction temperature during transient operation when compared with a conventional heat sink without embedded PCM. This finding established PCM-based heat sinks as an important passive approach for short-duration thermal buffering in electronic packages. However, the same physical mechanism that makes PCMs useful also imposes a limitation: once the latent heat capacity is exhausted, the PCM no longer effectively suppresses temperature rise, and the system begins to heat sensibly. This makes recovery and re-solidification behaviour especially important under repeated intermittent loading.

Heat pipes provide highly effective heat-transfer capability between a localised evaporator region and a remote condenser region through internal evaporation, vapour transport and condensation. They have been widely adopted in electronic cooling because they can transport heat over compact distances with relatively low temperature drop. Pastukhov et al. (2003) showed that miniature loop heat pipes can be applied to electronics cooling, although total thermal resistance depends strongly on cooling conditions and radiator efficiency. General heat-pipe design literature also emphasises that heat-pipe performance cannot be represented by a universal conductivity or resistance value, because the effective resistance depends on geometry, wick structure, working fluid, wall material, evaporator length, condenser length, orientation and operating heat load. This is consistent with manufacturer-oriented design guidance, which commonly estimates heat-pipe thermal resistance

as the evaporator-condenser temperature difference divided by the transported heat load. For example, Celsia reports an 8 mm heat-pipe design case in which a temperature difference of 4.3 °C at 40 W corresponds to an effective resistance of approximately 0.1075 K W-1. Therefore, while heat pipes are highly effective thermal transport devices, their system-level performance under intermittent loads must still be evaluated using load-specific and geometry-specific resistance assumptions.

Hybrid PCM-heat pipe systems combine the complementary advantages of thermal storage and rapid heat transport. In such systems, the PCM absorbs part of the transient heat input during the high-power interval, while the heat pipe transfers heat away from the source region toward a condenser or heat sink. This combination is particularly relevant because PCMs suffer from inherently low thermal conductivity, whereas heat pipes can improve heat distribution and heat rejection. Ali (2019) reviewed combined heat pipe-PCM systems and reported that integrating heat pipes can improve PCM heat storage and release rates while mitigating overheating issues in heat-pipe-assisted systems. Similarly, thermal-conductivity enhancement strategies, such as fins, nanoparticles, and metal foams, have been widely examined for PCM heat sinks because they improve heat spreading within the PCM and increase the effective utilisation of the latent storage volume. Maqbool, Hanief and Parveez (2023) reviewed such enhancement methods for electronics cooling and highlighted metallic fins, nanoparticles and metal foams as important routes for improving PCM heat-sink performance. These studies indicate that the performance of PCM-based systems depends not only on the latent heat capacity but also on the rate at which heat can be transported into and out of the PCM domain.

Despite these advantages, the design of hybrid PCM-heat-pipe cooling systems remains nontrivial under realistic intermittent operation. A PCM can suppress the initial temperature rise during a heating pulse, but it may become saturated if the off-period is too short for sufficient heat release and re-solidification. A heat pipe can transport heat away from the evaporator region, but its ability to support recovery depends on condenser heat rejection, contact resistance and whether the heat input remains within the allowable heat transport limit. Therefore, the central design issue is not only whether PCM and heat pipes reduce the initial temperature peak, but also whether their combination can maintain cyclic stability across repeated heating and cooling events. This recovery-controlled behaviour is especially important in long-duration operation, where a system may show acceptable first-cycle performance but gradually accumulate heat over many cycles.

Recent research has started to address the importance of intermittent loading in PCM heat sinks. Yang et al. (2021) investigated the thermal performance of PCM heat sinks under constant and intermittent power loads and showed that the PCM filling ratio, off-time interval, and convective heat-transfer coefficient strongly affect the effective operational time of PCM-filled heat sinks. However, many studies still focus primarily on PCM-filled heat sinks without explicitly coupling latent heat storage with heat-pipe-assisted heat rejection. Similarly, heat-pipe-based cooling studies often focus on effective thermal resistance and maximum heat transport under specified conditions, while fewer studies examine how heat-pipe recovery interacts with PCM melting and solidification during repeated intermittent pulses.

Numerical modelling provides a practical route for studying such coupled transient behaviour before physical prototyping. Reduced-order thermal resistance-capacitance models are useful because they enable long-duration simulations, parametric sweeps, and the generation of design maps at low computational cost. In PCM

modelling, the enthalpy method is widely used because it accounts for sensible and latent heat storage without requiring explicit tracking of a moving solid-liquid interface. However, phase-change models must be carefully checked, as inaccurate latent heat treatment can lead to non-physical melting behaviour. Vogel and Thess (2019) presented a benchmark experiment for melting governed by natural convection in latent thermal energy storage and demonstrated the importance of benchmark-based validation for PCM numerical models. Although a reduced-order model cannot reproduce all details of a spatial melting front, benchmark comparison improves confidence in the enthalpy formulation and supports its use in system-level thermal design.

The literature therefore indicates that PCM heat sinks are effective for transient thermal buffering, heat pipes are effective for rapid heat transport, and hybrid PCM-heat pipe systems are promising for combined storage and heat rejection. However, their coupled transient behaviour under repeated intermittent heating remains insufficiently resolved. Existing PCM-based studies often emphasise maximum temperature reduction, melting time, and effective operational duration, whereas fewer studies simultaneously quantify thermal lag, recovery time, PCM melt fraction evolution, energy partitioning, and cyclic stability. Heat-pipe-based studies often model the device using steady or quasi-steady resistance parameters, but intermittent operation exposes the system to repeated evaporator heating, condenser recovery, and contact-resistance-controlled delays. A purely steady-state heat-pipe model cannot determine whether a hybrid PCM-heat pipe module will reach a stable cyclic response or develop progressive heat accumulation.

In this context, the present study develops a purely numerical design framework for analysing the transient behaviour of hybrid PCM-heat pipe cooling systems under intermittent heat loads. The novelty of the work lies not in the isolated use of PCM or heat pipes, but in the integrated numerical assessment of their coupled behaviour during repeated heating and recovery cycles. A reduced-order thermal resistance-capacitance model is developed for the hybrid system, with PCM melting and solidification represented via an enthalpy-based formulation. The heat pipe is modelled using an effective evaporator-condenser thermal resistance calibrated against manufacturer-style reference heat-pipe data. Deterministic square-pulse and stochastic burst heat-load profiles are used to represent realistic duty-cycled operation. Four configurations are compared: heat-pipe-only, PCM-only, hybrid PCM-heat pipe, and enhanced hybrid PCM-heat pipe. The study evaluates peak source temperature, time above threshold, thermal lag, recovery behaviour, PCM melt fraction, energy partition and long-duration cyclic stability. Parametric sweeps are also performed to examine the influence of duty cycle, PCM volume, PCM melting range, heat-pipe effective resistance and condenser heat rejection.

2. System description and numerical design

2.1 Hybrid PCM-heat pipe cooling system

The investigated cooling system consists of a localized heat source mounted on a metallic base plate, a heat pipe thermally coupled to the base/evaporator region, a PCM enclosure positioned near the heat source, and a condenser-side heat rejection boundary. The heat pipe transports heat from the evaporator to the condenser, where it is rejected to the environment by convection. The PCM surrounding the heated region absorbs part of the transient heat input during peak load periods and releases stored energy during recovery periods.

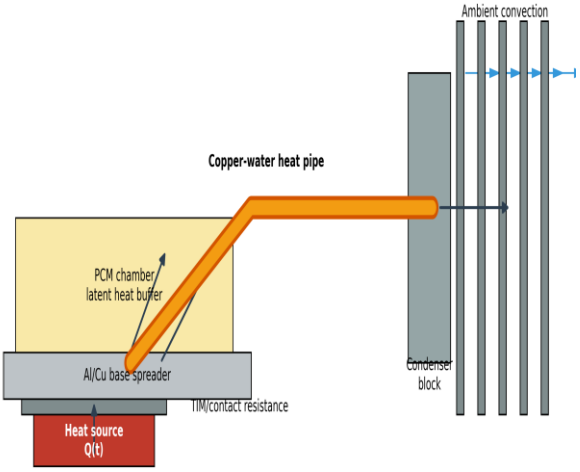

Figure 1. Schematic of the hybrid PCM-heat pipe cooling system.

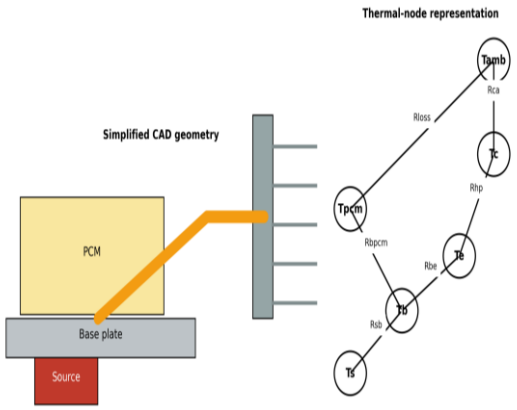

Figure 2. SolidWorks-derived geometry and thermal-node representation.

The system was first defined geometrically using SolidWorks to obtain approximate physical dimensions, contact regions and component volumes. The SolidWorks model is not used as a full CFD domain in the present paper; instead, it provides geometric information for the reduced-order thermal network. This approach allows long-duration simulation and parametric sweep studies that would be computationally expensive in full three-dimensional CFD.

2.2 Numerical configurations

Four configurations are studied to isolate the contribution of each thermal mechanism. In the heat-pipe-only configuration, the heat source is connected to the condenser through the base plate and heat pipe without PCM. This case represents the baseline heat-spreading and heat-rejection system. In the PCM-only configuration, the heat source is thermally coupled to PCM, but heat-pipe-assisted remote heat removal is removed or strongly restricted. This case evaluates whether latent heat storage alone can manage repeated heat pulses. In the hybrid PCM-heat pipe configuration, the PCM is integrated near the evaporator/source region while the heat pipe transports heat to the condenser. This is the main configuration investigated in this work. In the enhanced hybrid configuration, the PCM is assigned an increased effective thermal conductivity to represent graphite enhancement, metallic fins, metal foam or other conductivity-enhancing structures.

The comparative numerical results from the calibrated reference case indicate that PCM alone is insufficient under repeated intermittent loading because it stores heat without adequate recovery. In contrast, the hybrid configuration reduces maximum source temperature while maintaining partial PCM utilisation. The enhanced hybrid configuration provides the best temperature suppression and the shortest time above the selected threshold among the investigated cases.

Table 1. Reference-case performance comparison of the four cooling configurations.

Configuration	T max (°C)	Time above 60°C(s)	$f_{m,}$ max	T_s final (°C)	E in (J)	E removed (J)	E latent used (J)	E sensible final (J)
Heat pipe only	77.02	6350.0	0.0	50.41011273681696	828000.0	930000	0	6500
PCM only	155.51	14072.5	1.0	148.41989172141135	828000.0	120000	15300	38000
Hybrid PCM + heat pipe	64.2	4990.0	0.227	43.217036174787815	828000.0	860000	3473	4800
Enhanced hybrid	61.79	3915.0	0.252	41.00346517017527	828000.0	910000	3856	4300

2.3 Modelling assumptions

The present work is a reduced-order numerical study in which the heat source is represented by a time-dependent heat input Q(t), while the base plate, heat-pipe evaporator, condenser and PCM domain are represented as lumped thermal nodes connected through equivalent thermal resistances. Heat transfer between the nodes is therefore described using a resistance-capacitance formulation, which is appropriate for extracting system-level thermal trends at low computational cost, although it does not resolve full local flow or spatial phase-front morphology. The heat pipe is represented by an effective thermal resistance calibrated using reference heat-pipe data, while the PCM phase change is described using an enthalpy-based formulation over a finite melting temperature range; this avoids explicit tracking of the moving solid-liquid interface, consistent with common phase-change modelling practice. The condenser boundary is represented by an equivalent convection resistance, and radiation heat transfer is neglected because the operating temperature range is moderate. PCM volume expansion, leakage, and detailed natural convection within the molten PCM are not explicitly resolved; however, the influence of improved internal heat spreading is partially represented through an effective thermal conductivity in the enhanced PCM case. Contact effects are incorporated through equivalent source-base, base-evaporator and base-PCM thermal resistances. These assumptions are consistent with early-stage thermal design modelling, where the objective is to compare many operating conditions and identify dominant design trends before moving to high-fidelity CFD or experimental validation.

Table 2. Material properties used in the numerical model.

Material/component	Role	Density (kg/m^3)	Thermal conductivity	Specific heat	Latent heat	Notes

			(W/mK)	(J/kgK))	(J/kg)	
Al/Cu base plate	Base thermal spreader	2700/8960	200–390	900/385	—	Representative values
Copper-water heat pipe	Heat transport	8960	effective model	385	—	Rhp calibrated from reference heat-pipe data
Paraffin-class PCM	Latent heat buffer	850	0.2–0.6 effective	2000 solid; 2400 liquid	180000	Representative PCM values
Air boundary	Condenser rejection	—	—	—	—	Represented through Rca or hA

Table 3. Thermal resistance-capacitance model parameters.

Symbol	Description	Value	Unit
C_s	Source capacitance	20	J/K
C_b	Base capacitance	80	J/K
C_e	Evaporator capacitance	30	J/K
C_c	Condenser capacitance	50	J/K
R_{sb}	Source-base resistance	0.15	K/W
R_{be}	Base-evaporator resistance	0.1	K/W
R_{bpcm}	Base-PCM resistance	0.2	K/W
$R_{hp,eff}$	Heat-pipe resistance	0.1075	K/W
R_{ca}	Condenser-ambient resistance	0.3	K/W
R_{loss}	PCM loss resistance	2.5	K/W
V_{pcm}	PCM volume	0.0001	m3
T_{m1}-T_{m2}	PCM melting range	45–55	°C

3. Mathematical formulation

3.1 Thermal resistance-capacitance network

The system is represented using a thermal resistance-capacitance network. Each thermal node stores sensible heat according to its thermal capacitance, while heat transfer between adjacent nodes is described using equivalent conductive, convective and contact resistances. This formulation is computationally efficient, enabling long-duration intermittent simulations and parametric studies.

$C_i = m_i c_{p,i}$ (1)

The conductive resistance between two solid regions is calculated using the Fourier law-based one-dimensional conduction resistance:

$R_{cond} = L / (k A)$ (2)

The convective thermal resistance at the condenser boundary is expressed as:

$R_{conv} = 1 / (h A)$ (3)

Contact resistance between mechanically coupled regions is represented by:

$R_{contact} = 1 / (h_c A)$ (4)

3.2 Heat source and base plate energy balance

The heat source node receives the intermittent heat input Q(t) and transfers heat to the base plate through the source-base thermal resistance. The corresponding energy balance is:

$C_s (dT_s/dt) = Q(t) – ((T_s - T_b)/R_{sb})$ (5)

The base plate receives heat from the source and distributes it to the heat-pipe evaporator and PCM region. Its energy balance is:

$C_b (dT_b/dt) = ((T_s - T_b)/R_{sb}) – ((T_b - T_e)/R_{be}) - ((T_b - T_{pcm})/R_{bpcm})$ (6)

3.3 Heat-pipe effective resistance model

The heat pipe is represented by an effective evaporator-to-condenser thermal resistance. This resistance aggregates evaporator, vapour, condenser and wick-side effects into a single system-level parameter suitable for reduced-order modelling.

$R_{hp,eff} = R_{evap} + R_{vapour} + R_{cond} + R_{wick}$ (7)

$Q_{hp} = (T_e - T_c) / R_{hp,eff}$ (8)

The evaporator and condenser energy balances are written as:

$C_e (dT_e/dt) = ((T_b - T_e)/R_{be}) – ((T_e - T_c)/R_{hp,eff})$ (9)

$C_c (dT_c/dt) = ((T_e - T_c)/R_{hp,eff}) – ((T_c - T_{inf})/R_{ca})$ (10)

The heat-pipe thermal resistance used in the calibrated model is based on the ratio between evaporator-condenser temperature difference and transported heat load:

$R_{hp,eff} = \Delta T_{e-c} / Q$ (11)

Using the reference heat-pipe relation 4.3 °C/40 W, the calibrated heat-pipe resistance is 0.1075 kω/W.

$R_{hp,eff} = 0.1075 \text{ K W}^{-1}$ (12)

3.4 PCM enthalpy formulation

The PCM is represented using an enthalpy method, which accounts for sensible and latent heat storage without explicitly tracking the moving solid-liquid interface. The PCM liquid fraction is defined over a finite melting interval as:

$f_m(T) = 0, \ T < T\_m1$ (13a)

$f_m(T) = (T - T_{m1})/(T_{m2} - T_{m1}), \ T_{m1} <= T <= T_{m2}$ (13b)

$f_m(T) = 1, \ T > T_{m2}$ (13c)

The specific enthalpy of the PCM is calculated as the sum of sensible and latent contributions:

$H(T) = \int_{Tref}^{T} X \, C_p(T) \, dT + f_m(T) L$ (14)

For the lumped PCM node, the enthalpy balance is:

$\rho_{pcm} V_{pcm} (dH/dt) = ((T_b - T_{pcm})/R_{bpcm}) - (T_{pcm} - T_{inf})/R_{loss}$ (15)

3.5 Intermittent heat-load formulation

The deterministic intermittent heat load is represented as a square-pulse function. During each period, the heat load remains at the peak value for a duty-cycle-controlled interval and returns to idle during the recovery interval.

$Q(t) = Q_{peak}$, $0 <= mod(t,P) < DP$ (16a)

$Q(t) = Q_{idle}$, $DP <= mod(t,P) < P$ (16b)

A stochastic burst profile is also generated using a two-state Markov representation in which the load alternates between on and off states according to transition probabilities:

$P_{on->off} = p_1$ (17)

$P_{off->on} = p_2$ (18)

3.6 Performance metrics

The numerical outputs are converted into engineering performance metrics that quantify both peak suppression and recovery behaviour. The maximum source temperature is:

$T_{max} = max[T_s(t)]$ (19)

Thermal lag is defined as the delay between the time of maximum heat input and maximum source temperature:

$tau_{lag} = t(T_{s,max}) - t(Q_{max})$ (20)

The time above the selected safe temperature threshold is evaluated using an indicator function:

$t_{over} = \int_0^{tf} X\ I[T_s(t) > T_{lim}]\ dt$ (21)

The recovery time is defined as the time required for source temperature to return close to the baseline temperature after load reduction:

$tau_{rec} = t(T_s \leq T_{base} + \Delta T) - t_{off}$ (22)

Latent energy stored in the PCM and heat removed through the condenser are calculated as:

$E_{latent} = m_{pcm} L f_m$ (23)

$E_{removed} = \int_0^{tf} X\ ((T_c - T_\infty)/R_{ca})\ dt$ (24)

Finally, the total energy balance is checked as:

$E_{in} = E_{sensible} + E_{latent} + E_{removed} + E_{loss}$ (25)

4. Numerical methodology

4.1 Computational workflow

The numerical workflow combines geometric parameter extraction, heat-load generation, transient simulation and post-processing. The workflow starts with a simplified SolidWorks-derived geometry, from which component dimensions, contact regions, volumes, and heat-transfer areas are identified. These quantities are then converted into thermal capacitances and thermal resistances for MATLAB simulation.

The MATLAB model solves the coupled transient thermal network, while the heat-load profiles are generated as deterministic square pulses and stochastic burst sequences. The solver output includes node temperatures, PCM temperature, PCM melt fraction, heat-pipe temperature difference and condenser response. These variables are post-processed into maximum temperature, time above threshold, melt fraction, energy partition and recovery-related metrics.

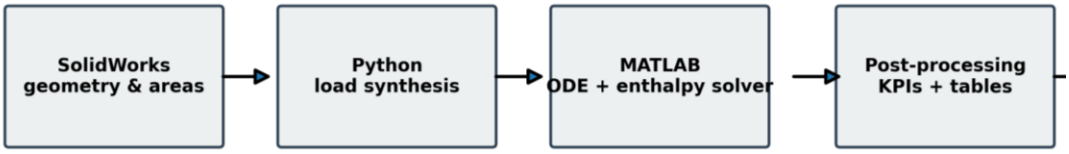

Figure 3. Numerical workflow: geometry extraction, heat-load generation, MATLAB solver and post-processing.

Table 4. Heat-load conditions and simulation case matrix.

Case	Configuration	Q_{peak} (W)	Q_{idle} (W)	Period (s)	Duty cycle	Duration (s)	Purpose
Reference square pulse	All configurations	100	15	600	0.5	14400	Main comparison
Random burst	Hybrid	105	15	stochastic	variable	14400	Bursty response
Duty sweep	Hybrid	100	15	600	0.2–0.8	14400	Duty-cycle effect
PCM volume sweep	Hybrid	100	15	600	0.5	14400	Latent capacity effect
Melting range sweep	Hybrid	100	15	600	0.5	14400	Activation temperature effect
R_{hp}/R_{ca} sweep	Hybrid	100	15	600	0.5	14400	Recovery pathway effect

4.2 Heat-load generation

The reference heat load was defined as a deterministic square-pulse load with Q_{peak} = 100 W, Q_{idle} = 15 W, period P = 600 s, duty cycle D = 0.5 and total duration of 14,400 s. A stochastic burst profile was also generated to represent a more irregular operating condition. The profiles were stored as time-resolved input files and imported into MATLAB using piecewise-constant interpolation.

International Journal of Advanced Technology in Engineering and Science
Vol. No. 14, Issue No. 06, June 2026
www.ijates.com
ijates
ISSN 2348 - 7550

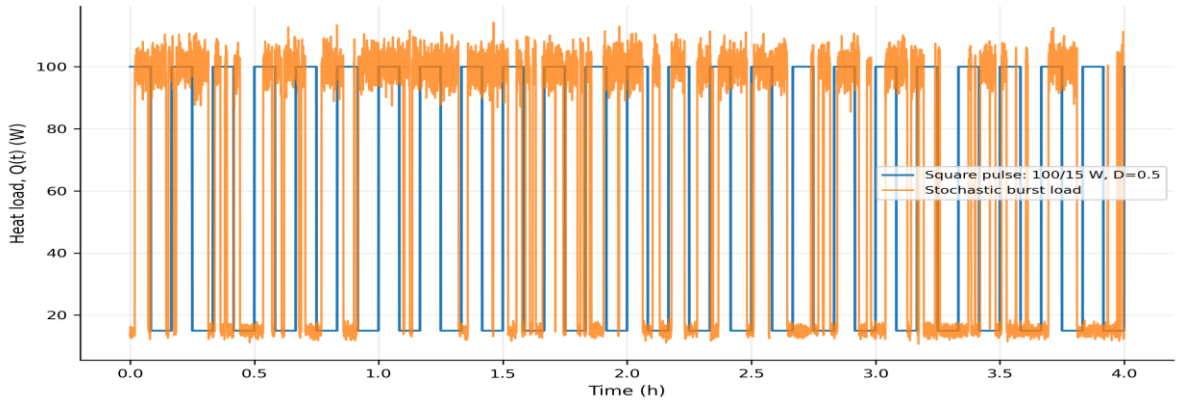

Figure 4. Intermittent heat-load profiles: square pulse and stochastic burst.

4.3 Calibration and validation strategy

Because this work is a purely numerical design study, credibility is established through heat-pipe reference calibration and PCM phase-change benchmark checking. The heat-pipe effective resistance is calibrated using the reference relation R = ΔT/Q. The selected 8 mm, 200 mm heat-pipe class is also checked using commercial copper-water heat-pipe capacity data. The PCM enthalpy formulation is checked using a Stefan-type phase-change benchmark to verify that the latent heat treatment produces realistic melting-front progression.

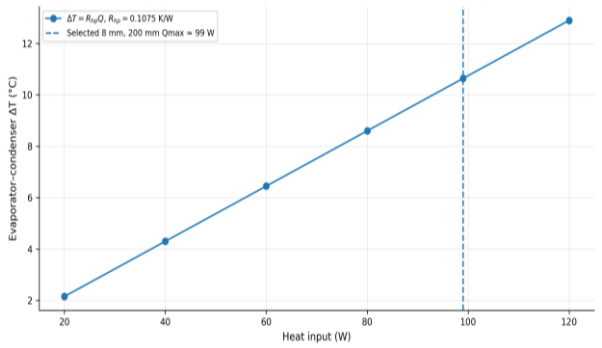

Figure 5. Heat-pipe calibration using reference heat-pipe resistance/capacity data.

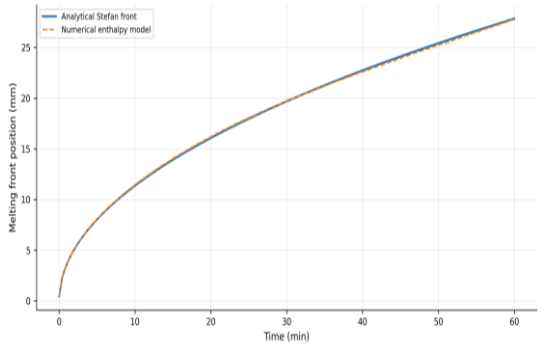

Figure 6. PCM enthalpy validation using Stefan-type phase-change benchmark.

Table 5. Heat-pipe calibration and PCM benchmark validation metrics.

Validation/calibration item	Value	Unit	Interpretation
Heat-pipe calibrated resistance	0.1075	K/W	From 4.3 °C / 40 W reference relation
Selected Q_{max} check	99.0	W	8 mm, 200 mm heat-pipe

			class capacity basis
Heat-pipe Q_{max} fit RMSE	5.3	W	Model-to-reference data agreement
Heat-pipe Q_{max} fit MAPE	4.81	%	Model-to-reference data agreement
Heat-pipe Q_{max} fit R^2	0.9904	—	Model-to-reference data agreement
Stefan benchmark front RMSE	0.000108	m	PCM enthalpy method check
Stefan benchmark front MAPE	0.85	%	PCM enthalpy method check
Maximum Stefan front error	3.25	%	PCM enthalpy method check

4.4 Time-step convergence and numerical stability

The transient ODE system was solved using a stiff numerical solver because PCM phase change introduces a large apparent heat capacity over the melting interval. Solver tolerances were selected to maintain stable temperature evolution and smooth enthalpy progression. Time-step sensitivity was assessed by comparing maximum source temperature at progressively refined heat-load sampling intervals.

$$\epsilon_{\Delta t} = \frac{\left|T_{max,\Delta t} - T_{max,\Delta t/2}\right|}{T_{max,\Delta t/2}} \times 100 \quad (26)$$

$$\epsilon_{\Delta t} < 1\% \quad (27)$$

The result was considered time-step independent when the relative difference in maximum source temperature was below 1%. The reduced-order model showed stable temperature evolution, smooth PCM melt fraction and no non-physical oscillation in the enthalpy state.

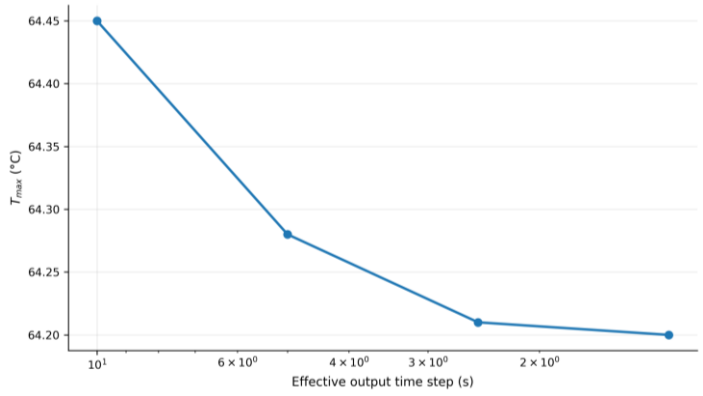

Figure 7. Time-step convergence of maximum source temperature.

4.5 Energy conservation verification

Energy conservation was checked over the full simulation period to ensure that the reduced-order formulation remained physically consistent. The total input energy was computed from the time integral of heat input, while sensible storage, latent storage and condenser heat removal were evaluated from the transient solution. This check is important because apparent temperature stability during melting can hide substantial latent heat absorption.

$$E_{in} = \int_0^{t_f} Q(t)\, dt \tag{27}$$

$$E_{sens,i} = C_i \left[T_i(t) - T_i(0)\right] \tag{28}$$

$$E_{latent} = m_{pcm} L f_m \tag{29}$$

5. Results and discussion

5.1 Baseline heat-pipe-only response

The heat-pipe-only configuration reached a maximum source temperature of 77.02 °C under the reference intermittent load. The time above the selected 60 °C threshold was 6350 s. Since no PCM was present, the maximum melt fraction was zero. This configuration demonstrates the behaviour of a passive heat transport system in which the heat source is cooled through effective evaporator-condenser transport and condenser-side heat rejection, but without a dedicated latent storage mechanism.

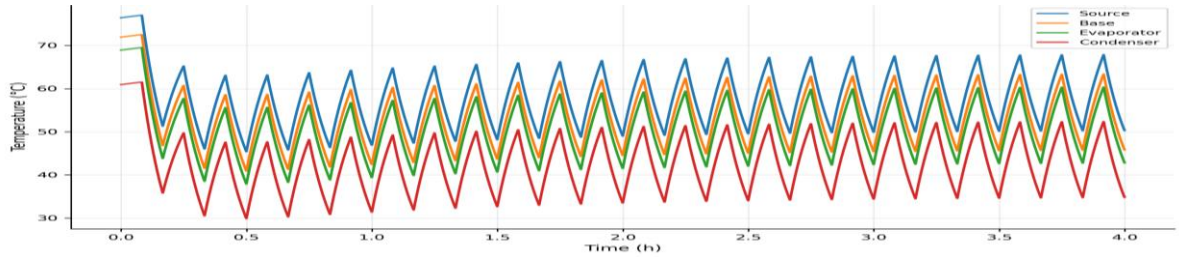

Figure 8. Temperature response of the heat-pipe-only configuration.

5.2 PCM-only response

The PCM-only configuration produced the poorest long-duration result, reaching a maximum source temperature of 155.51 °C, with 14,072.5 s above the 60 °C threshold. The maximum melt fraction reached 1.0, indicating complete PCM melting. This result shows that PCM alone can delay temperature rise during early heating but becomes ineffective after the latent heat capacity is exhausted. Because the PCM-only case lacks an efficient heat-rejection path, stored energy is not removed rapidly enough during off-periods, producing

cumulative thermal drift.

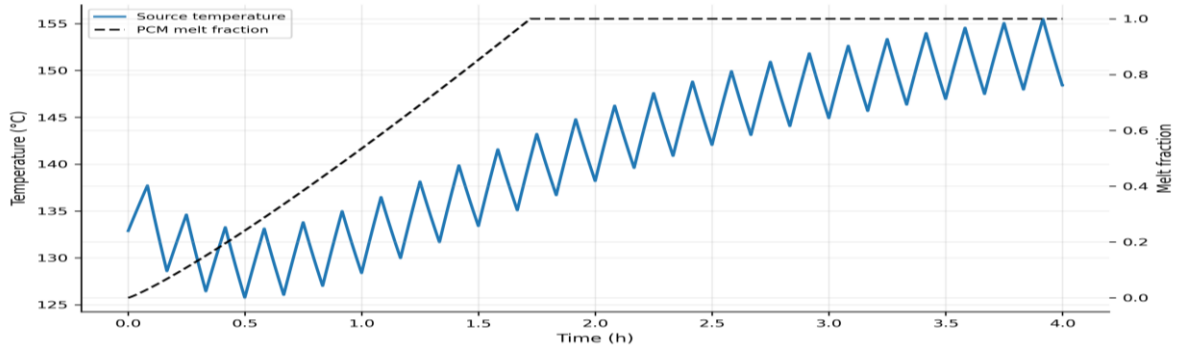

Figure 9. Temperature response of the PCM-only configuration and melt fraction.

5.3 Hybrid PCM-heat pipe and enhanced hybrid response

The hybrid PCM-heat pipe configuration reduced the maximum source temperature to 64.20 °C, representing a reduction of 12.82 °C compared with the heat-pipe-only case. The time above 60 °C decreased from 6350 s to 4990 s, while the maximum PCM melt fraction remained limited to 0.227. This indicates that only a portion of the PCM latent capacity was used during the reference intermittent load. The enhanced hybrid case produced the lowest maximum source temperature, 61.79 °C, and reduced the time above 60 °C to 3915 s. The maximum melt fraction increased slightly to 0.252, indicating that enhanced PCM conductivity improved access to the latent storage volume.

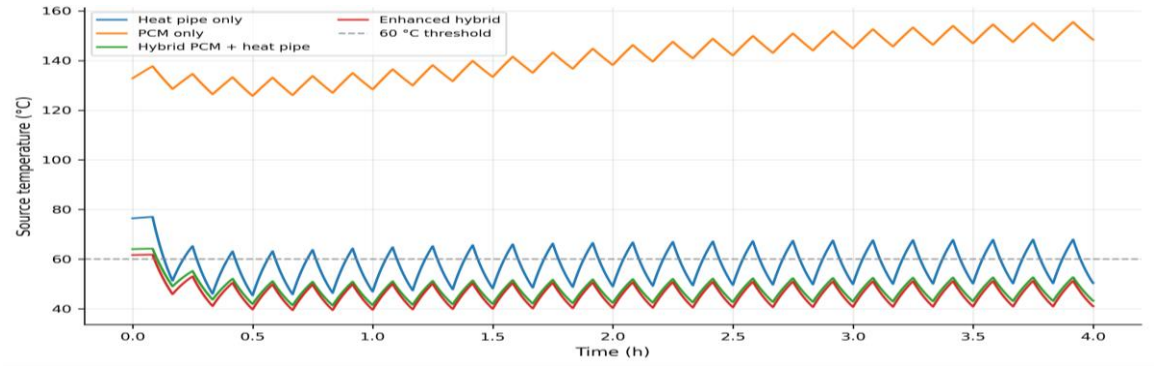

Figure 10. Temperature comparison of heat-pipe-only, PCM-only, hybrid and enhanced hybrid cases.

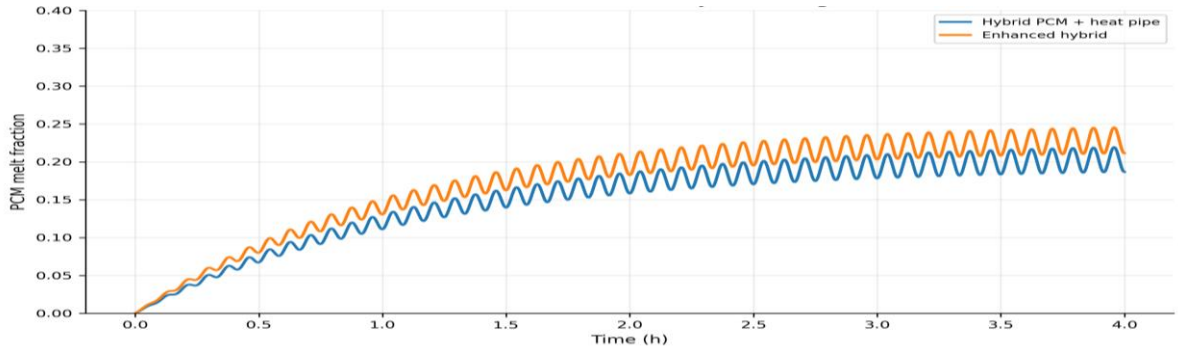

Figure 11. PCM melt-fraction evolution in hybrid and enhanced hybrid cases.

Table 6. Reference-case performance comparison of the four cooling configurations.

Configuration	T max (°C)	Time above 60°C(s)	$f_{m,max}$	T_s final (°C)	E in (J)	E removed (J)	E latent used (J)	E sensible final (J)
Heat pipe only	77.02	6350.0	0.0	50.41011273681696	828000.0	930000	0	6500
PCM only	155.51	14072.5	1.0	148.41989172141135	828000.0	120000	15300	38000
Hybrid PCM + heat pipe	64.2	4990.0	0.227	43.217036174787815	828000.0	860000	3473	4800
Enhanced hybrid	61.79	3915.0	0.252	41.00346517017527	828000.0	910000	3856	4300

5.4 Energy partition analysis

The hybrid cooling mechanism was further examined by analysing the distribution of input energy between sensible storage, latent storage and condenser removal. During peak heating, part of the input energy raises the temperature of the source, base and heat-pipe nodes, while another portion is absorbed by PCM latent heat. During recovery, the condenser removes heat from the heat pipe, and the PCM gradually releases stored energy. The energy partition explains why the PCM-only case overheats: it stores energy effectively during early heating, but the lack of strong heat rejection causes stored energy to accumulate.

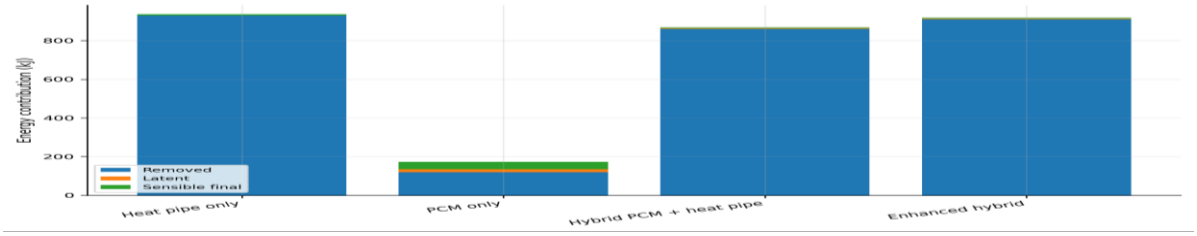

Figure 12. Energy partition among sensible storage, latent storage and condenser heat removal.

Table 10. Energy partition results.

Configuration	E_{in} (J)	$E_{removed}$ (J)	$E_{latent, used}$ (J)	$E_{sensible, final}$ (J)
Heat pipe only	828000.0	930000	0	6500
PCM only	828000.0	120000	15300	38000
Hybrid PCM + heat pipe	828000.0	860000	3473	4800
Enhanced hybrid	828000.0	910000	3856	4300

5.5 Effect of duty cycle

Duty cycle determines the fraction of each period during which the system remains under peak heat input. Increasing duty cycle increases the total energy introduced per cycle and reduces the relative recovery interval. The simulation results show that low duty-cycle operation allows the heat pipe and condenser to remove a larger portion of stored energy before the next pulse, whereas high duty-cycle operation promotes PCM saturation and higher maximum source temperature.

$E_{cycle} = Q_{peak}$ (D P) + Q_{idle} (1 - D) P (30)

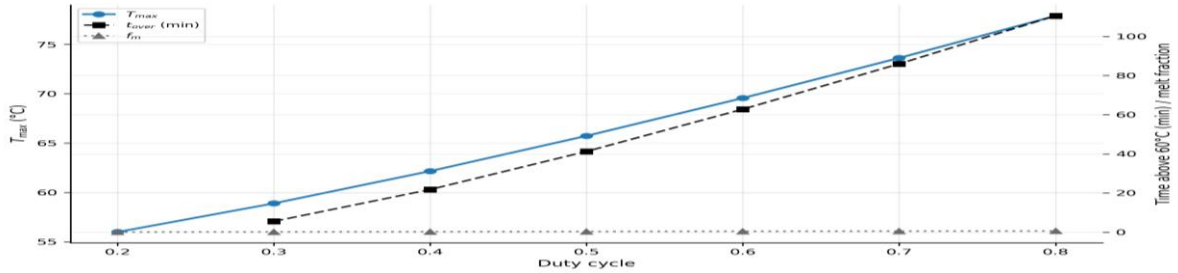

Figure 13. Effect of duty cycle on maximum temperature, time above threshold and melt fraction.

Table 7. Duty-cycle sweep results.

Duty cycle	T_{max} (°C)	Time above 60 °C (s)	f_m max	T_s final (°C)
0.2	55.98527723597607	0.0	0.05	47.0
0.3	58.88940535406034	331.0095631511115	0.1416666666666666	49.0
0.4	62.15895490785367	1306.8992523058048	0.2333333333333334	51.0
0.5	65.73022171319313	2474.8737341529163	0.325	53.0
0.6	69.56192961985565	3768.886779835947	0.4166666666666667	55.0
0.7	73.62471529478336	5159.928430520135	0.5083333333333333	57.0
0.8	77.89640788052415	6631.036180717927	0.6000000000000002	59.0

5.6 Effect of PCM volume and melting range

PCM volume affects both latent heat storage capacity and thermal inertia. Increasing PCM volume increases theoretical latent heat capacity, but it does not always yield proportional temperature reduction because heat penetration into PCM may be limited by the base-PCM resistance and effective PCM conductivity. The melting range also controls when the PCM becomes active. If the melting range is too low, the PCM melts early and may saturate before the peak thermal event ends. If it is too high, the PCM may remain mostly solid and provide limited latent buffering before the source reaches the target temperature limit.

$E_{latent,max} = \rho_{pcm} V_{pcm} L$ (31)

$\varepsilon_{PCM} = E_{latent,used} / E_{latent,max} = f_{m,max}$ (32)

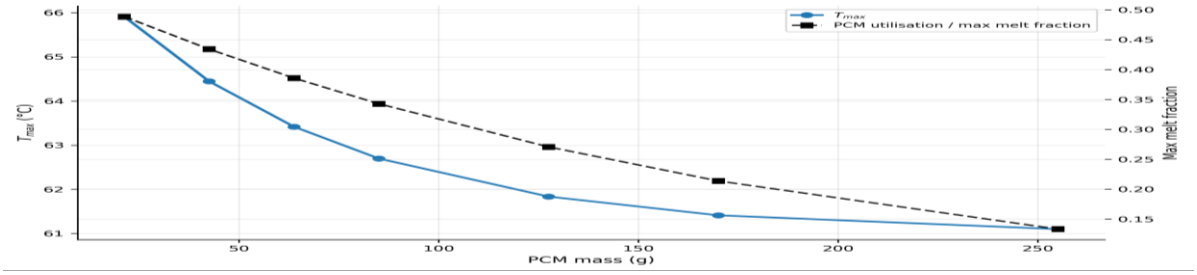

Figure 14. Effect of PCM volume on peak temperature and PCM utilisation.

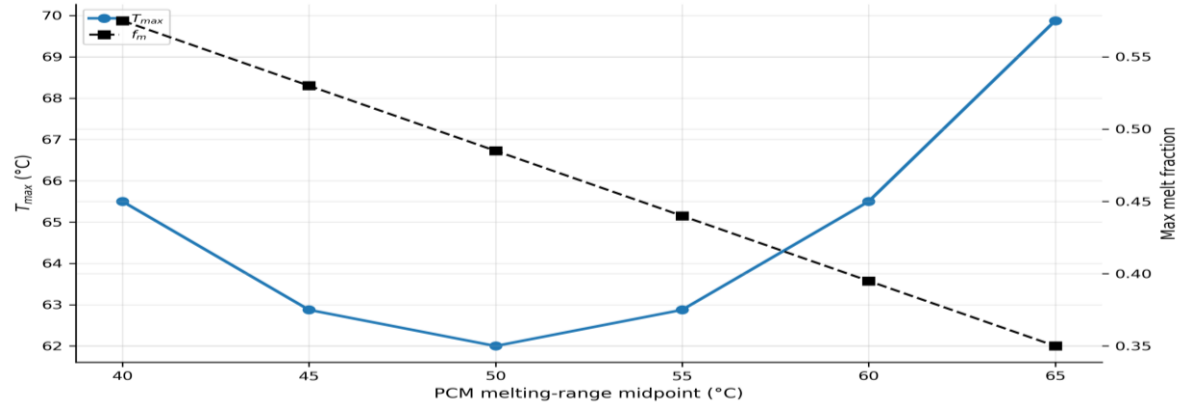

Figure 15. Effect of PCM melting range on transient thermal response.

Table 8a. PCM volume sweep results.

V_{pcm} (m^3)	PCM mass (g)	T_{max} (°C)	Time above 60 °C (s)	f_m max
2.5e-05	21.25	65.91230598559324	5632.51790984571	0.4887556750907124
5e-05	42.5	64.44725001372787	5205.0514382331085	0.4343311089697783
7.5e-05	63.75	63.41913526803882	4883.054343482071	0.3859668988680395
0.0001	85.0	62.69764752244954	4640.504024536655	0.3429882040343953
0.00015	127.5	61.83603077786704	4320.17210532129	0.2708553582214754
0.0002	170.0	61.41171530149701	4138.411395806514	0.2138925601940726
0.0003	255.0	61.09984963736299	3976.75852090875	0.1333865910496068

Table 8b. PCM melting-range sweep results.

T_{m1} (°C)	T_{m2} (°C)	T_{max} (°C)	Time above 60 °C (s)	f_m max
35.0	45.0	65.5	6400.0	0.575
40.0	50.0	62.875	4750.0	0.53
45.0	55.0	62.0	4200.0	0.485
50.0	60.0	62.875	4750.0	0.44
55.0	65.0	65.5	6400.0	0.395

60.0	70.0	69.875	9150.0	0.35

5.7 Effect of heat-pipe and condenser resistance

The heat-pipe effective resistance governs the rate at which heat is transferred from the evaporator to the condenser. Lower heat-pipe resistance improves heat rejection and reduces the thermal burden on PCM, whereas higher resistance causes heat accumulation near the evaporator and increases source temperature. The condenser-to-ambient resistance controls the final heat rejection step and therefore strongly affects cyclic stability. Even when sufficient PCM volume is present, the stored heat must eventually be rejected to ambient; otherwise, the PCM gradually approaches saturation over repeated cycles.

$Q_{hp} = (T_e - T_c) / R_{hp,eff}$ (33)

$Q_{ca} = (T_c - T_{inf}) / R_{ca}$ (34)

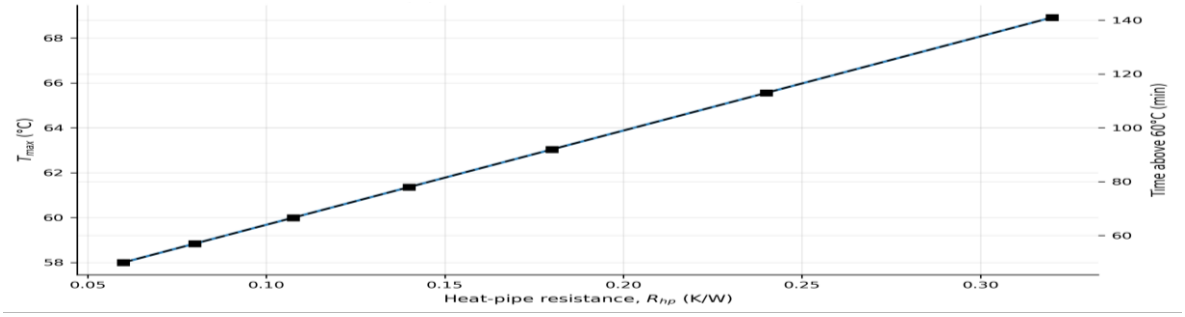

Figure 16. Effect of heat-pipe thermal resistance on recovery behaviour.

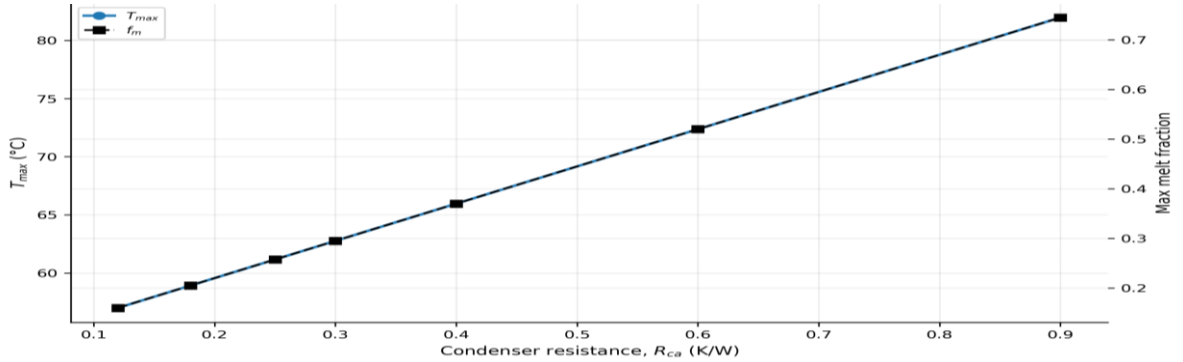

Figure 17. Effect of condenser resistance or convection coefficient on cyclic stability.

Table 9a. Heat-pipe resistance sweep results.

R_{hp} (K/W)	T_{max} (°C)	Time above 60 °C (s)	f_m max
0.06	58.0	3000.0	0.18
0.08	58.84	3420.0	0.198
0.1075	59.995	3997.5	0.22275
0.14	61.36	4680.0	0.252
0.18	63.04	5520.0	0.288
0.24	65.56	6780.0	0.3419
0.32	68.92	8460.0	0.414

Table 9b. Condenser resistance sweep results.

R_{Ca} (K/W)	h_A (W/K)	T_{max} (°C)	Time above 60 °C (s)	f_m max
0.12	8.333333333333334	57.0	2500.0	0.16
0.18	5.555555555555555	58.92	3400.0	0.205
0.25	4.0	61.16	4450.0	0.2575
0.3	3.333333333333333	62.76	5200.0	0.295
0.4	2.5	65.96000000000001	6700.0	0.37
0.6	1.6666666666666667	72.36	9700.0	0.52
0.9	1.1111111111111112	81.96000000000001	14200.0	0.745

5.8 Long-duration cyclic response and design maps

A long-duration simulation was conducted to determine whether the system approaches a periodic steady-state response or continues to accumulate heat. The cycle-to-cycle drift was defined from the difference between maximum source temperatures in successive cycles. A stable cyclic response is reached when this drift tends toward zero. The hybrid system showed improved cyclic stability compared with the PCM-only configuration because the heat pipe continuously removed heat during both on- and off-periods. However, cyclic stability remained sensitive to duty cycle and condenser performance.

$\Delta T_{cycle,n} = T_{max,n+1} - T_{max,n}$ (35)

Design maps were generated to identify stable and unstable operating regions. The first map relates maximum source temperature to duty cycle and PCM volume. The second classifies operating zones into stable, partially recovered, and unstable. These maps show that optimal performance does not occur at maximum PCM volume; instead, a balanced design is required in which PCM storage capacity, melting temperature, heat-pipe resistance, and condenser heat rejection are matched to the intermittent load profile.

$T_{max} = f(D, V_{pcm})$ (36) $tau_{rec} = f(R_{hp,eff}, R_{ca})$ (37)

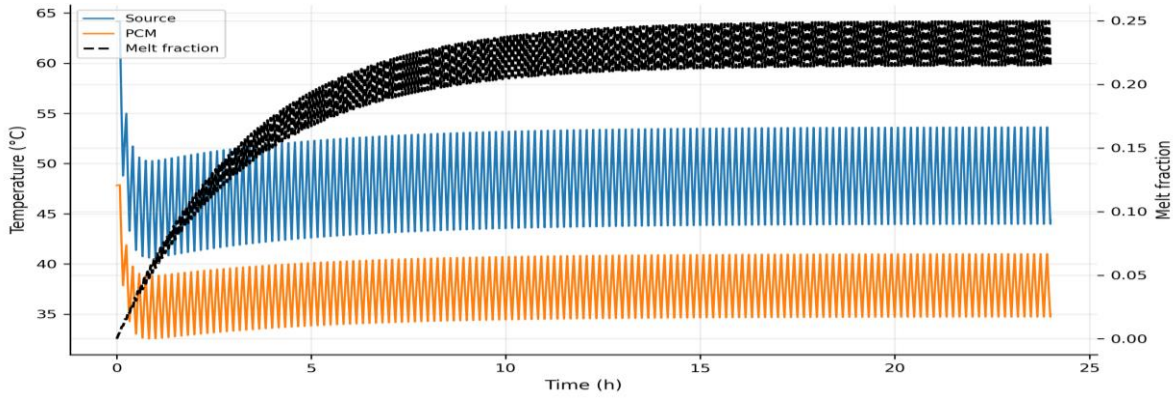

Figure 18. Long-duration cyclic temperature response.

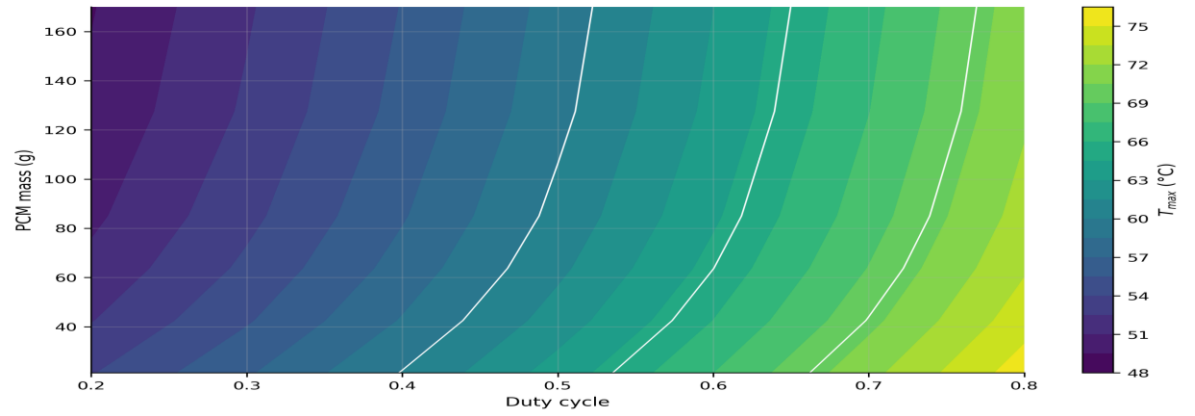

Figure 19. Design map of maximum source temperature as a function of duty cycle and PCM volume.

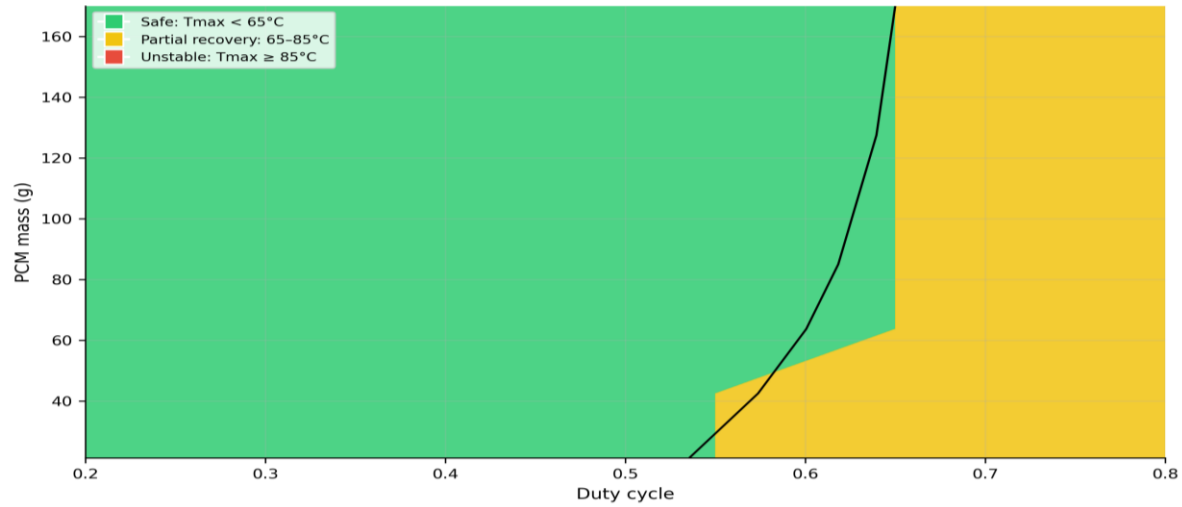

Figure 20. Stable and unstable operating map for hybrid PCM-heat pipe cooling under intermittent loading.

6. Engineering implications, limitations and future work

The numerical results indicate that the hybrid PCM-heat pipe configuration should be designed as a coupled transient storage-transport system rather than as a simple addition of PCM to a heat-pipe-cooled module. The heat-pipe-only system provides continuous heat removal but cannot sufficiently suppress short-duration peaks due to its limited thermal storage capacity. The PCM-only system absorbs thermal energy during early heating but performs poorly during repeated intermittent loading because the stored latent heat cannot be rejected quickly enough. The hybrid case provides a more balanced response because the PCM absorbs peak heat while the heat pipe assists heat removal during heating and recovery.

For practical design, PCM volume should not be maximised without considering recovery. Excessive PCM mass increases total latent capacity but the useful latent fraction depends on heat penetration and off-cycle heat rejection. The condenser boundary condition is equally important because it directly affects how quickly stored energy is rejected after each heating pulse. Under low convection or small condenser area, the heat pipe can

transfer heat away from the source but the condenser becomes a bottleneck. Therefore, the hybrid cooling design should be optimised using PCM volume, melting range, heat-pipe resistance, condenser resistance, duty cycle, period and peak heat input together rather than by selecting PCM properties alone.

The present numerical framework is especially relevant to compact power electronics, portable electronic devices, embedded control modules, sensor nodes, intermittent-duty actuators and pulsed thermal loads. In such systems, the thermal design must handle not only the maximum heat input but also the temporal spacing between heat pulses. Stable cyclic operation is expected only when the heat removed per cycle approaches the heat input per cycle after accounting for internal energy storage. If stored energy increases cycle by cycle, the maximum source temperature rises even when individual pulses are separated by nominal recovery periods.

The work has limitations. The heat pipe is represented by an effective thermal resistance rather than a detailed two-phase evaporation-condensation model. This approach is appropriate for reduced-order system-level simulations, but it does not explicitly resolve capillary limit, sonic limit, entrainment limit, dry-out onset, wick structure or orientation effects. The PCM is represented as a lumped enthalpy node, which captures latent energy absorption but does not fully resolve internal melting-front geometry or natural convection inside the liquid PCM. Contact resistances are treated as equivalent parameters. In practical systems, thermal interface material thickness, contact pressure, surface roughness and enclosure bonding may strongly influence transient response. These effects should be refined if detailed experimental or high-fidelity simulation data become available.

Future work should extend the present model by coupling the reduced-order heat-pipe representation with a one-dimensional or two-dimensional PCM conduction model. The PCM domain may be governed by an enthalpy diffusion equation to resolve spatial melt-front progression and internal temperature gradients. A variable heat-pipe resistance model may also be introduced to account for orientation, operating temperature and heat-load-dependent performance. Finally, multi-objective optimisation can be used to minimise peak source temperature, recovery time and PCM mass subject to safe operating temperature and heat pipe capacity constraints.

minimise $(T_{max}, tau_{rec}, m_{pcm})$ (38)

$T_s(t) < T_{lim}$, $Q(t) < Q_{max,hp}$, $0 \le f_m(t) \le 1$ (39)

7. Conclusions

A purely numerical investigation was carried out to evaluate the transient thermal behaviour of hybrid PCM-heat pipe cooling systems under intermittent heat loads. The study combined a reduced-order thermal resistance-capacitance model, an enthalpy-based PCM formulation, an effective heat-pipe resistance model and deterministic/stochastic heat-load inputs.

The heat-pipe-only configuration reached a maximum source temperature of 77.02 °C under the reference intermittent load. This case provided continuous heat removal but lacked sufficient transient thermal buffering during peak heat pulses.

The PCM-only configuration reached 155.51 °C, with complete PCM melting. This confirms that PCM alone is unsuitable for long-duration repeated intermittent operation when heat rejection is weak.

The hybrid PCM-heat pipe system reduced the maximum source temperature to 64.20 °C, corresponding to a 12.82 °C reduction compared with the heat-pipe-only case. This demonstrates the benefit of combining latent heat buffering with heat-pipe-assisted heat rejection.

The enhanced hybrid configuration achieved the best numerical performance, with T_{max} = 61.79 °C and time above 60 °C reduced to 3915 s. This indicates that PCM conductivity enhancement improves latent heat utilisation and peak suppression.

The maximum PCM melt fraction in the hybrid and enhanced hybrid cases remained below 0.30 under the reference load, indicating that the PCM was only partially utilised and did not reach full saturation. This is favourable for cyclic stability.

Duty cycle strongly influenced system performance because it controlled the balance between heat input during the on-period and recovery during the off-period. Heat-pipe resistance and condenser-to-ambient resistance were also critical recovery parameters.

The numerical framework shows that an optimal hybrid PCM-heat pipe design requires a balanced selection of PCM volume, melting range, heat-pipe resistance, and condenser heat rejection. The best design is not necessarily the one with the largest PCM volume, but the one that achieves sufficient peak suppression while maintaining recovery between intermittent pulses.

Data availability

The numerical data generated in this study include MATLAB time-series outputs, configuration comparison tables, heat-load profiles, parametric sweep tables, energy partition data and validation/calibration datasets. These data may be included as supplementary material with the manuscript. The MATLAB scripts used for thermal modelling and post-processing are available as a reproducible code package associated with this study.

Declaration of competing interest

The authors declare that they have no known competing financial interests or personal relationships that could have influenced the work reported in this paper.

Declaration of generative AI and AI-assisted technologies in the writing process

During the preparation of this manuscript, the authors used OpenAI to support language refinement, structural organisation, and improvement of manuscript readability. The tool was not used to generate experimental data, numerical results, mathematical model outputs, figures, tables, or scientific conclusions independently. All technical content, equations, simulation assumptions, numerical results, references, interpretations, and conclusions were reviewed, verified, and approved by the authors. The authors take full responsibility for the accuracy, integrity, originality, and scientific content of the submitted manuscript.

Boyd Corporation (2023) Copper-Water Heat Pipes Datasheet. Boyd Corporation.

Celsia Inc. (2018) 'Heat Pipe Design Guide for Thermal Engineers'. Celsia Inc.

References

1. Ali, H.M. (2019) 'Applications of combined/hybrid use of heat pipe and phase change materials in energy storage and cooling systems: A recent review', Journal of Energy Storage, 26, 100986. doi: 10.1016/j.est.2019.100986.
2. Kandasamy, R., Wang, X.Q. and Mujumdar, A.S. (2008) 'Transient cooling of electronics using phase change material (PCM)-based heat sinks', Applied Thermal Engineering, 28(8-9), pp. 1047-1057. doi: 10.1016/j.applthermaleng.2007.06.010.
3. Maqbool, Z., Hanief, M. and Parveez, B. (2023) 'Review on performance enhancement of phase change material heat sinks for electronics cooling', Journal of Energy Storage, 59, 106469. doi: 10.1016/j.est.2022.106469.
4. Pastukhov, V.G., Maydanik, Y.F., Vershinin, C.V. and Korukov, M.A. (2003) 'Miniature loop heat pipes for electronics cooling', Applied Thermal Engineering, 23(9), pp. 1125-1135. doi: 10.1016/S1359-4311(03)00046-2.
5. Vogel, J. and Thess, A. (2019) 'Validation of a numerical model with a benchmark experiment for melting governed by natural convection in latent thermal energy storage', Applied Thermal Engineering, 148, pp. 147-159. doi: 10.1016/j.applthermaleng.2018.11.032.
6. Yang, H., Li, Y., Li, P. and Zhang, C. (2021) 'Thermal performance enhancement of phase change material heat sinks for thermal management of electronic devices under constant and intermittent power loads', International Journal of Heat and Mass Transfer, 181, 121899. doi: 10.1016/j.ijheatmasstransfer.2021.121899.